Numerical Bifurcation Analysis of Delay Differential Equations Using DDE-BIFTOOL

K. ENGELBORGHS, T. LUZYANINA, and D. ROOSE
Katholieke Universiteit Leuven

We describe DDE-BIFTOOL, a Matlab package for numerical bifurcation analysis of systems of delay differential equations with several fixed, discrete delays. The package implements continuation of steady state solutions and periodic solutions and their stability analysis. It also computes and continues steady state fold and Hopf bifurcations and, from the latter, it can switch to the emanating branch of periodic solutions. We describe the numerical methods upon which the package is based and illustrate its usage and capabilities through analysing three examples: two models of coupled neurons with delayed feedback and a model of two oscillators coupled with delay.

Categories and Subject Descriptors: G.1.0 [**Numerical analysis**]: General—*numerical algorithms*; G.1.4 [**Numerical analysis**]: Quadrature and Numerical Differentiation; G.1.7 [**Numerical analysis**]: Ordinary Differential Equations—*multistep and multivalue methods*; G.4 [**Mathematical software**]—*algorithm design and analysis*

General Terms: Algorithms

Additional Key Words and Phrases: Continuation, delay differential equations, numerical stability and bifurcation analysis, software package

1. INTRODUCTION

DDE-BIFTOOL is a collection of Matlab routines for numerical bifurcation analysis of systems of delay differential equations (DDEs) with multiple fixed,

This paper concerns version 1.00 of the package. Version 2.00 (which also supports the computation of homoclinic and heteroclinic solutions and the analysis of state-dependent delay equations) is compatible with version 1.00 and became available [Engelborghs et al. 2001] after this manuscript was submitted. This research presents results of the research project OT/98/16, funded by the Research Council K. U. Leuven, of the research project G.0270.00 funded by the Fund for Scientific Research-Flanders (Belgium) and of the research project IUAP P4/02 funded by the Programme on Interuniversity Poles of Attraction, initiated by the Belgian State, Prime Minister's Office for Science, Technology and Culture. The scientific responsibility is assumed by its authors. K. Engelborghs is a Postdoctoral Fellow of the Fund for Scientific Research-Flanders (Belgium).
Authors' address: Department of Computer Science, Katholieke Universiteit Leuven, Celestijnenlaan 200A, B-3001 Heverlee-Leuven, Belgium; T. Luzyanina on leave from the Institute of Mathematical Problems in Biology, Puschino, Moscow region, 142290, Russia; email: {Koen.Engelborghs;Tatyana.Luzyanina;Dirk.Roose}@cs.kuleuven.ac.be.

discrete delays. It is freely available for scientific purposes [Engelborghs 2000a]. The package can be used to compute branches of steady state solutions and steady state fold and Hopf bifurcations using continuation. Given an equilibrium, it approximates the rightmost, stability determining roots of the characteristic equation which can further be corrected using a Newton's iteration. Periodic solutions and their Floquet multipliers are computed using orthogonal collocation with adaptive mesh selection. Branches of periodic solutions can be continued starting from a previously computed Hopf point or an initial guess of a periodic solution.

The DDE-BIFTOOL package is the first package of this kind, and as such, it can encourage the use of time delays in modelling. Software packages already exist only for simulation (time integration) of delay differential equations, such as ARCHI [Paul 1997], DKLAG6 [Corwin et al. 1997] and XPPAUT [Ermentrout 1998]. A more complete list of available software for DDEs (with links) is included at the webpage of the package [Engelborghs 2000a]. Only two packages deal with some form of stability analysis: XPPAUT allows limited stability analysis of steady state solutions of DDEs using the approach described in Luzyanina and Roose [1996] and the program BIFDD [Hassard 1987] allows normal form analysis of Hopf bifurcation points provided good starting values are available.

In this paper we outline the numerical methods upon which DDE-BIFTOOL is based and illustrate its usage and capabilities by a number of examples. We comment on the choice of method parameters, the accuracy of the results and possible problems that can occur. We assume the reader is familiar with the basic notions of bifurcation analysis (see e.g. Seydel [1994]; Kuznetsov [1995]; Govaerts [2000] in the context of ordinary differential equations) and with the basic theory on delay differential equations (see e.g. Hale and Verduyn Lunel [1993]; Diekmann et al. [1995]; Kolmanovskii and Myshkis [1999]). The remainder of the paper is structured as follows. Some necessary notations and properties of delay differential equations are briefly described in Section 2. Descriptions of the numerical methods are given in Section 3. Results of the analysis of three systems of DDEs and accompanying remarks on using the package are given in Section 4. We conclude with some brief remarks on limits to the package and future plans in Section 5.

2. NOTATIONS AND NECESSARY BACKGROUND

Consider the system of delay differential equations,

$$\frac{\mathrm{d}}{\mathrm{d}t}x(t) = f(x(t), x(t-\tau_1), \ldots, x(t-\tau_m), \eta), \tag{1}$$

where $x(t) \in \mathbb{R}^n$, $f : \mathbb{R}^{n(m+1)} \times \mathbb{R}^p \to \mathbb{R}^n$ is a nonlinear smooth function depending on a number of (time-independent) parameters $\eta \in \mathbb{R}^p$, and delays $\tau_i > 0$, $i = 1, \ldots, m$. Call τ the maximal delay,

$$\tau := \max_{i=1,\ldots,m} \tau_i.$$

A solution $x(t)$ of (1) on $t \in [0, \infty)$ is uniquely defined by specifying as initial condition a function segment, $x(\theta) = x_0(\theta),\ -\tau \le \theta \le 0$.

The linearization of (1) around a solution $x^*(t)$ is the *variational equation* given by Hale [1977]

$$\frac{\mathrm{d}}{\mathrm{d}t} y(t) = A_0(t) y(t) + \sum_{i=1}^{m} A_i(t) y(t - \tau_i), \tag{2}$$

where, using $f \equiv f(x^0, x^1, \ldots, x^m, \eta)$,

$$A_i(t) := \left. \frac{\partial f}{\partial x^i} \right|_{(x^*(t), x^*(t-\tau_1), \ldots, x^*(t-\tau_m), \eta)}, \quad i = 0, \ldots, m. \tag{3}$$

If $x^*(t)$ corresponds to a steady state solution,

$$x^*(t) \equiv x^* \in \mathbb{R}^n, \quad \text{with } f(x^*, x^*, \ldots, x^*, \eta) = 0,$$

then the matrices $A_i(t)$ are constant, $A_i(t) \equiv A_i$, and the corresponding variational equation (2) leads to a *characteristic equation*. Define the $n \times n$-dimensional matrix Δ as

$$\Delta(x^*, \eta, \lambda) := \lambda I - A_0 - \sum_{i=1}^{m} A_i \mathrm{e}^{-\lambda \tau_i}. \tag{4}$$

The characteristic equation, obtained by substituting the sample eigensolution $y(t) = v\mathrm{e}^{-\lambda t}$ in (2) and seeking for nonzero solutions, then reads,

$$\det(\Delta(x^*, \eta, \lambda)) = 0. \tag{5}$$

Equation (5) has an infinite number of roots $\lambda \in \mathbb{C}$ called the *characteristic roots*, which determine the local stability of the steady state solution x^*. The steady state solution is (asymptotically) stable provided all characteristic roots have negative real part; it is unstable if there exists a root with positive real part. It is known that the number of characteristic roots in any half plane $\Re(\lambda) > \gamma$, $\gamma \in \mathbb{R}$, is finite [Hale 1977]. Hence, the stability is always determined by a finite number of roots.

Bifurcations occur whenever characteristic roots move through the imaginary axis as one or more parameters are changed. Generically two types of bifurcations occur in a one parameter continuation of steady state solutions: a fold bifurcation (or turning point) where the steady state branch turns in parameter space, and where a real characteristic root passes through zero; and a Hopf bifurcation where a branch of periodic solutions originates, and where a pair of complex conjugate characteristic roots crosses the imaginary axis.

A periodic solution $x^*(t)$ is a solution which repeats itself after a finite time, that is,

$$x^*(t + T) = x^*(t), \quad \text{for all } t.$$

Here $T > 0$ is the period. If the function f is arbitrarily smooth then (unlike a general solution of (1)) a periodic solution is arbitrarily smooth due to its periodicity and the smoothing property of the solution operator of (1).

The stability of the periodic solution is determined by the spectrum of the time integration operator $S(T, 0)$ which integrates the variational equation (2) around $x^*(t)$ from time $t = 0$ to $t = T$. This operator is called the *monodromy operator* and its (infinite number of) eigenvalues, which are independent of the starting moment $t = 0$, are called the *Floquet multipliers*. Furthermore, if $T \geq \tau$ then $S(T, 0)$ is compact [Hale 1977].

For autonomous systems, there is always a *trivial* Floquet multiplier at 1, corresponding to a perturbation along the periodic solution. The periodic solution is stable provided all multipliers (except the trivial one) have modulus smaller than 1; it is unstable if there exists a multiplier with modulus larger than 1. Bifurcations occur whenever Floquet multipliers move into or out of the unit circle. Generically three types of bifurcations occur in a one parameter continuation of periodic solutions: a turning point where the branch turns in parameter space and where a real multiplier crosses through 1; a period doubling point where a period-doubled branch of periodic solutions originates and where a real multiplier crosses through -1; and a torus bifurcation where a branch of quasi-periodic solutions originates and where a complex pair of multipliers crosses the unit circle.

3. NUMERICAL METHODS

In this section we describe the numerical methods that are implemented in the package. More details on these methods can be found in the articles Luzyanina and Roose [1996], Engelborghs and Roose [1999], Engelborghs et al. [2000a], Engelborghs and Roose [2001], and in Engelborghs [2000b]. A comparison of these methods to previously developed methods for numerical analysis of DDEs can be found in Engelborghs et al. [2000b].

Below we describe the determining systems whose solution points are (or approximate) the solutions we are interested in (comparable to corresponding ones used in, e.g., Doedel et al. [1997]). Newton's iteration is then used to compute these solutions and we mention the number of free parameters necessary to obtain isolated solution points under generic conditions. We describe the computation of the stability of the computed point. Finally, we briefly comment on the computation of branches of solution points in function of an extra parameter by use of a continuation procedure.

3.1 Steady State Solutions

First, we describe the computation and stability analysis of steady state solutions and their generic codimension-1 bifurcations.

3.1.1 *Determining Systems.* A steady state solution $x^* \in \mathbb{R}^n$ of (1) is determined from $(n \times n)$-dimensional determining system with no free parameters (i.e. η is fixed),

$$f(x^*, x^*, \ldots, x^*, \eta) = 0. \tag{6}$$

Fold bifurcations are determined from the following $(2n + 1) \times (2n + 1)$-dimensional determining system using one free parameter (i.e. one component

of η is treated as an extra unknown and allowed to vary during Newton iterations),

$$\begin{cases} f(x^*, x^*, \ldots, x^*, \eta) = 0 \\ \Delta(x^*, \eta, 0)v = 0 \\ c^{\mathrm{T}}v - 1 = 0. \end{cases} \tag{7}$$

Here, Δ is the characteristic matrix (4) evaluated at $\lambda = 0$. The vector $v \in \mathbb{R}^n$ is introduced to avoid the use of a determinant in (7). At convergence, v is a null-vector of Δ. $c^{\mathrm{T}}v - 1 = 0$ represents a suitable normalisation of v. The vector $c \in \mathbb{R}^n$ is chosen as $c = v^{(0)}/(v^{(0)^{\mathrm{T}}}v^{(0)})$, where $v^{(0)}$ is the initial value for v.

Hopf bifurcations are determined from the following $(2n + 1) \times (2n + 1)$-dimensional complex determining system using one free parameter (one component of η),

$$\begin{cases} f(x^*, x^*, \ldots, x^*, \eta) = 0 \\ \Delta(x^*, \eta, \mathrm{i}\omega)v = 0 \\ c^{\mathrm{H}}v - 1 = 0. \end{cases} \tag{8}$$

At convergence, $v \in \mathbb{C}^n$ is an eigenvector of Δ corresponding to $\lambda = \mathrm{i}\omega$, where $\omega \in \mathbb{R}$ represents the Hopf frequency. The vector $c \in \mathbb{C}^n$ is chosen as $c = v^{(0)}/(v^{(0)^{\mathrm{H}}}v^{(0)})$. Note that the partially complex system (8) can be written as a $(3n+2) \times (3n+2)$ real system in the unknowns $x^* \in \mathbb{R}^n$, $\Re(v) \in \mathbb{R}^n$, $\Im(v) \in \mathbb{R}^n$, one component of η and $\omega \in \mathbb{R}$.

For each determining system we mentioned the number of free parameters necessary to obtain generically isolated solutions. If additional conditions are appended to these systems, a corresponding extra number of parameters should be freed. This ensures the use of square Jacobians during Newton's iteration, which (for well chosen conditions and free parameters) generically have isolated solutions. If, on the other hand, the number of free parameters and added conditions are not appropriately matched then Newton's iteration solves systems with a non-square Jacobian. In this case (for safety reasons signalled by a warning message), Matlab uses an over- or under-determined least squares procedure. This approach can be useful in some situations (e.g. when symmetries are present in the system, cf. Section 4.1).

3.1.2 *Roots of the Characteristic Equation.* Once a steady state solution is obtained, stability is determined by computing the rightmost roots of its characteristic equation. These roots are first approximated using a linear multistep method (LMS-method) applied to (2).

Consider the linear k-step LMS-formula [Hairer et al. 1993],

$$\sum_{j=0}^{k} \alpha_j y_{L+j} = h \sum_{j=0}^{k} \beta_j f_{L+j}, \tag{9}$$

applied to the variational equation (2). Here, $\alpha_k = 1$, $h > 0$ is a (fixed) step size, y_j and f_j,

$$f_j = A_0 y_j + \sum_{i=1}^{m} A_i \tilde{y}(t_j - \tau_i), \tag{10}$$

present numerical approximations of $y(t)$ respectively $A_0 y(t)+\sum_{i=1}^{m} A_i y(t-\tau_i)$ at the mesh point $t_j := jh$ (assuming $t_0 = 0$ is used as a starting point). The approximations $\tilde{y}(t_j - \tau_l)$ (where $t_j - \tau_l$ may or may not be a mesh point) are obtained from interpolating through several y_i in the past, $i < j$. In particular, the use of so-called Nordsieck interpolation leads to

$$\begin{aligned} \tilde{y}(t_j - \tau_l) = \tilde{y}(t_i + \epsilon h) = \sum_{\nu=-s_-}^{s_+} P_\nu(\epsilon) y_{i+\nu}, \quad \epsilon \in [0,1), \\ \text{with } P_\nu(\epsilon) := \prod_{k=-s_-, k\neq\nu}^{s_+} \frac{\epsilon - k}{\nu - k}, \end{aligned} \tag{11}$$

the Lagrange polynomials through the points $-s_-, \ldots, s_+$ and where s_- respectively s_+ represent the number of interpolation points taken to the left respectively to the right of $t_j - \tau_l$.

To avoid using mesh points with index greater than $L + k$ we require that $\min \tau_i \geq s_+ h$. The resulting method is explicit whenever $\beta_k = 0$ and $\min \tau_i \geq (s_+ + 1)h$. That is, y_{L+k} can then directly be computed from (9) by evaluating

$$y_{L+k} = -\sum_{j=0}^{k-1} \alpha_j y_{L+j} + h \sum_{j=0}^{k-1} \beta_j f_{L+j},$$

whose right hand side depends only (through (10), (11)) on y_j, $j < L + k$.

The stability of the difference scheme thus obtained can easily be evaluated by computing the eigenvalues μ of the (linear) map between $[y_{L_{\min}} \cdots y_{L+k-1}]$ and $[y_{L_{\min}+1} \cdots y_{L+k}]$ where $L_{\min} = L - s_- - \lceil \tau/h \rceil$ is the smallest index used and where the mapping is defined by (9)–(11) for y_{L+k} and a shift for all other variables. If the eigenvalues μ all have modulus smaller than 1, the trajectories computed by the LMS-method converge to zero. If eigenvalues exist with modulus greater than one, trajectories exist which grow unbounded.

The LMS-method defines an approximation of $S(h, 0)$ (the time integration operator over the time step h). Hence, the eigenvalues μ approximate the eigenvalues of $S(h, 0)$ which are exponential transforms of the roots λ of the characteristic equation (5),

$$\mu = \exp(\lambda h). \tag{12}$$

(In addition $S(h, 0)$ may have some extra eigenvalues at zero [Hale 1977].) Hence, once μ is found, λ can be extracted using,

$$\Re(\lambda) = \frac{\ln(|\mu|)}{h}. \tag{13}$$

The imaginary part of λ is found modulo π/h, using

$$\Im(\lambda) \equiv \frac{\arcsin\left(\frac{\Im(\mu)}{|\mu|}\right)}{h} \left(\mathrm{mod} \frac{\pi}{h}\right), \quad \Im(\lambda) \in \left[-\frac{\pi}{2h}, \frac{\pi}{2h}\right]. \tag{14}$$

For small h, $0 < h \ll 1$, the smallest representation in (14) is assumed to be the most accurate one (that is, we let arcsin map into $[-\pi/2, \pi/2]$).

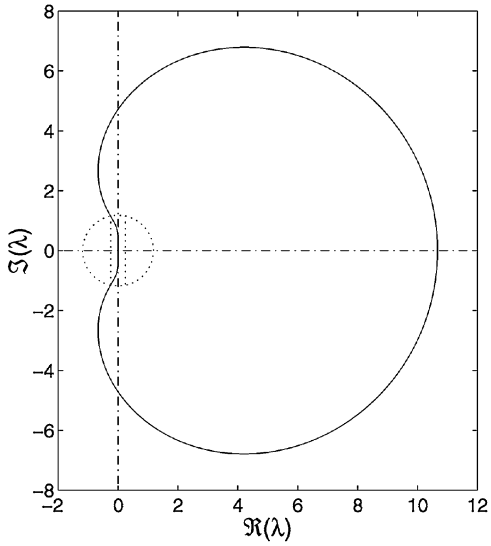

Fig. 1. Stability region (—) of the implicit 4th order backwards differentiation (BDF) LMS-method. Within a circle with radius $\rho_{\mathrm{LMS},\epsilon}$, except possibly in a band of size 2ϵ around the imaginary axis $(\cdots)$, stability is captured correctly by the LMS-method. Here, $\epsilon = 0.25$ was taken rather large for a clear visualisation. This method is used by default in the package with $\epsilon = 0.01$.

For reasons of stability, the parameters s_- and s_+ in formula (11) are chosen such that $s_- \leq s_+ \leq s_- + 2$, see Hong-Jiong and Jiao-Xun [1996]. Note that we want to approximate an infinite number of characteristic roots λ with a finite number of approximations (whose number depends on the size of h). However, there are only a finite number of rightmost, stability-determining characteristic roots, see Section 2. In Engelborghs and Roose [2001] it is shown that the steplength heuristic,

$$h = 0.9 \frac{\rho_{\mathrm{LMS},\epsilon}}{\|A_0\| + |r| + \sum_{i=1}^{m} \|A_i\| \mathrm{e}^{-r\tau_i}}, \tag{15}$$

can be used to approximate the (finite number of) roots with real part greater than a given $r < 0$, $\Re(\lambda) \geq r$ (implying also that h is small enough such that in (14) the appropriate choice of branch of the complex logarithm is taken). Here $\rho_{\mathrm{LMS},\epsilon}$ denotes, to some accuracy ϵ, a 'size of correctness' of the stability region of the LMS-method used, see Figure 1. For practical reasons, h is further bounded from below and above, see Section 4.1.

Approximations for the rightmost roots λ obtained from the LMS-method using (13), (14) can be corrected using a Newton iteration on the determining system

$$\begin{cases} \Delta(\lambda) v = 0 \\ c^{\mathrm{H}} v - 1 = 0. \end{cases} \tag{16}$$

As starting value for v, the eigenvector of $\Delta(\lambda)$ corresponding to the smallest eigenvalue (in modulus) is used.

Note that the collection of successfully corrected roots presents more accurate yet less robust information than the set of uncorrected roots. Indeed, attraction domains of roots of equations like (16) can be very small and hence corrections may diverge or approximations of different roots may be corrected to a single 'exact' root thereby missing part of the spectrum (as demonstrated in Section 4.1). Hence it is most safe to compare the approximations with their corrections.

3.2 Periodic Solutions

3.2.1 *Collocation.* A periodic solution is represented by the parameter values η, the period T, and the segment $x^*(t/T)$ on a mesh in [0, 1]. The mesh is an ordered collection of *interval points* $\{0 = t_0 < t_1 < \cdots < t_L = 1\}$ and *representation points* $t_{i+\frac{j}{d}}$, $i = 0, \ldots, L-1$, $j = 1, \ldots, d-1$, where

$$t_{i+\frac{j}{d}} = t_i + \frac{j}{d}(t_{i+1} - t_i).$$

The solution is approximated by a continuous piecewise polynomial on the mesh. More specifically, it is approximated by a polynomial of degree d on each subinterval $[t_i, t_{i+1}]$, $i = 0, \ldots, L-1$,

$$u(t) = \sum_{j=0}^{d} u\left(t_{i+\frac{j}{d}}\right) P_{i,j}(t), \quad t \in [t_i, t_{i+1}], \tag{17}$$

where $P_{i,j}(t)$ are the Lagrange polynomials through the points $t_{i+\frac{j}{d}}$, $j = 0, \ldots, d$. The approximation $u(t)$ is completely determined in terms of the coefficients

$$u_{i+j/d} := u\left(t_{i+j/d}\right), \quad i = 0, \ldots, L-1, \quad j = 0, \ldots, d-1 \quad \text{and} \quad u_L := u(t_L). \tag{18}$$

Because polynomials on adjacent intervals share the value at the common interval point, this representation is automatically continuous (it is, however, not continuously differentiable).

The collocation points are obtained as

$$c_{i,j} = t_i + c_j(t_{i+1} - t_i), \quad i = 0, \ldots, L-1, \quad j = 1, \ldots, d,$$

from a set of *collocation parameters* c_j, $j = 1, \ldots, d$. By default, the latter are chosen as the roots of the d-th degree Gauss-Legendre polynomial transformed to [0, 1].

A periodic solution (for a fixed value of the parameters η) is found as a solution $(u(s), s \in [0, 1]; T \in \mathbb{R})$ of the following $(n(Ld+1)+1) \times (n(Ld+1)+1)$-dimensional system in terms of the unknowns (18) and T,

$$\begin{cases} \dot{u}(c_{i,j}) = T f(u(c_{i,j}), u((c_{i,j} - \frac{\tau_1}{T}) \bmod 1), \ldots, u((c_{i,j} - \frac{\tau_m}{T}) \bmod 1), \eta) = 0, \\ \qquad\qquad i = 0, \ldots, L-1, \ j = 1, \ldots, d \\ u_0 = u_L \\ p(u) = 0. \end{cases} \tag{19}$$

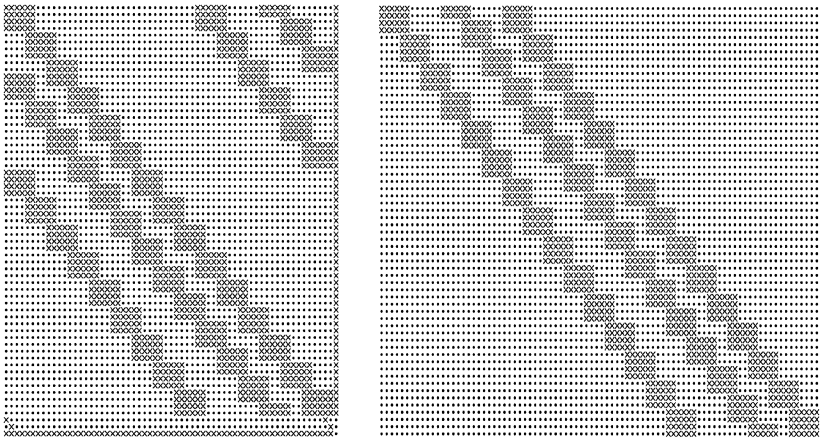

Fig. 2. Left: Sparse matrix structure of the linearization of (19): Zero elements $(\cdot)$, nonzero elements $(\times)$ for a fictitious periodic solution with $n = 2$, $\tau_1 = 8$, $\tau_2 = 3$ and $T = 20$; using $d = 2$ and an equidistant mesh on $[0, 1]$ with $L = 15$ subintervals. Right: Structure of the matrix used in the computation of the Floquet multipliers on a mesh in $[-\tau/T, 1]$ corresponding to the Jacobian in the left figure.

Here, p represents the classical integral phase condition [Doedel et al. 1991b] needed to remove translational invariancy,

$$\int_0^1 \dot{u}^{(0)}(s)\big(u^{(0)}(s) - u(s)\big)\,\mathrm{d}s = 0,$$

where $u^{(0)}$ is the initial solution of the Newton iteration and u the current solution.

In other words, the collocation solution is asked to fulfill the time-scaled differential equation exactly at the collocation points. Note that the piecewise polynomial u has a discontinuous derivative at the interval points. If $c_{i,j}$ coincides with t_i then the right derivative is taken in (19); if it coincides with t_{i+1} then the left derivative is taken. In other words the derivative taken at $c_{i,j}$ is that of u restricted to $[t_i, t_{i+1}]$.

The convergence rate of the maximal continuous error, $E = \max_{t\in[0,1]} \|u(t) - u^*(t)\|$ (where u^* is the exact solution), was proven to be $\mathcal{O}(h^d)$ in general and $\mathcal{O}(h^{d+1})$ for Gauss-Legendre collocation points on uniform and nonuniform meshes with $h = \max_i h_i$, $h_i = t_{i+1} - t_i$ [Engelborghs and Doedel 2001]. Special convergence at the interval points (the so-called superconvergence) known for ordinary differential equations, is, in general, lost for DDEs [Engelborghs et al. 2000a].

Adaptive mesh selection can be used to decrease the required number of intervals L for difficult profiles (with steep gradients). For the latter, the subinterval size h_i is adapted to an approximation of the $(d + 1)$-th derivative of the solution (obtained from the computed solution, see Ascher et al. [1988]; Engelborghs et al. [2000a]).

When an equidistant mesh is used, the linear systems arising during Newton's iteration on (19) have a sparsity pattern as visualised in Figure 2

(left). The current implementation does not exploit this sparsity. Note that when nonuniform meshes are used, the sparsity pattern becomes less regular, see Engelborghs et al. [2000a].

3.2.2 *Floquet Multipliers.* Floquet multipliers are computed as eigenvalues of the discretised time integration operator $S(T, 0)$. The discretization is obtained using the collocation equations (19) without the modulo operation and without phase and periodicity conditions. From this extended system on a mesh in $[-\tau/T, 1]$ (as in Figure 2 (right)) a discrete, linear map is obtained between the variables representing the segment $[-\tau/T, 0]$ and those representing the segment $[1 - \tau/T, 1]$. If these variables overlap, part of the map is constructed as just a time shift.

Convergence of computed Floquet multipliers for DDEs is studied in Luzyanina and Engelborghs [2001]. Some test results are given in Section 4.2.

3.3 Continuation

During continuation, a branch is computed by a combination of predictions and corrections (see, e.g. Seydel [1994]; Doedel et al. [1991a]). A new continuation point is predicted based on previously computed points using secant prediction over an appropriate steplength. The prediction is then corrected using the determining systems (6), (7), (8) or (19), bordered with a steplength condition which requires orthogonality of the correction to the secant vector. Hence one extra free parameter is necessary compared to the number of free parameters mentioned in Sections 3.1 and 3.2.

The following continuation and steplength determination strategy is used. If the last point was successfully computed, the steplength is multiplied with a given, constant factor greater than 1. If corrections diverged or if the corrected point was rejected because its accuracy was not acceptable, a new point is predicted, using linear interpolation, halfway between the last two successfully computed branch points. If the correction of this point succeeds, it is inserted in the branches point array at the correct position (before the previously last computed point). If the correction of the interpolated point fails again, the last successfully computed branch point is rejected (to avoid a possible branch switch) and the interpolation procedure is repeated between the (new) last two branch points.

This procedure ensures that after a failure (provided the interpolation procedure succeeds), the steplength is effectively divided by a factor two. Also, through inserting a newly computed point in between the last two computed points, the secant extrapolation direction is changed, which is not the case when using only secant extrapolation with steplength control.

3.4 Extra Conditions

The package allows the addition of extra conditions and corresponding free parameters to the determining systems presented earlier. We mention three possible applications of such extra conditions, two of which will be illustrated in Section 4.

First of all, extra conditions permit the continuation of branches in a larger parameter space with (possibly nonlinear) dependence between some parameters. A branch of steady state solutions can be continued by varying two parameters η_1, η_2 under the condition $\eta_1^2 + \eta_2^2 = 1$.

Second, it is possible to follow solutions satisfying some special property. A branch of homoclinic bifurcations can be approximated by following a branch of periodic solutions of large period. In this case, the period can be fixed at a large value using one extra condition and one additional parameter is freed (see Section 4.1).

Third, specific properties of a given system may cause the existence of special solutions which can still be computed using some substitution, an extra free parameter and an extra condition. This situation occurs, for example, with phase shifts in oscillators and will be explained in Section 4.3.

Note that these situations differ from the case of a system of differential-algebraic equations. In this case, the algebraic equations are part of the system definition and determine the stability together with the differential equations. In our application extra conditions are used to select special solutions of the (given) differential system.

4. EXAMPLES

DDE-BIFTOOL hides, as much as possible, its numerical methods and details from the user. For example, default method parameters can be obtained, some of which adapt automatically during continuation. We comment on these parameters and illustrate typical results and their accuracy by analysing three examples. For the analysis of steady state solutions, no parameters need to be user-chosen. For periodic solutions, the user needs to specify the degree of collocation polynomial and the size of the meshes used. Typically, one uses Gauss-Legendre collocation points (default), degrees $d = 3, 4$, and adaptive meshes with different number of subintervals, $L = 20, 40, \ldots, 160$ (starting from low values and going to higher values as difficulties are encountered).

4.1 Example 1

As a first illustrative example we use the following system of delay differential equations, taken from Shayer and Compbell [2000],

$$\begin{cases} \dot{x}_1(t) = -\kappa x_1(t) + \beta \tanh(x_1(t-\tau_s)) + a_{12} \tanh(x_2(t-\tau_2)) \\ \dot{x}_2(t) = -\kappa x_2(t) + \beta \tanh(x_2(t-\tau_s)) + a_{21} \tanh(x_1(t-\tau_1)). \end{cases} \tag{20}$$

This system models two coupled neurons with time delayed connections. We fix the parameters $\kappa = 0.5$, $\beta = -1$, $a_{12} = 1$ and $\tau_1 = \tau_2 = 0.2$ and vary a_{21} and τ_s.

It is clear that (20) has a trivial steady state solution $(x_1^*, x_2^*) = (0, 0)$ for all values of the parameters. We fix $a_{21} = 2.5$ and $\tau_s = 1.5$ and compute the rightmost roots of the characteristic equation at the zero steady state solution—see Figure 3. The solution is unstable due to the presence of a real characteristic root at $\lambda \approx 0.4223$. By default, the characteristic roots are approximated and corrected up to $\Re(\lambda) \geq -\frac{1}{\tau}$. A different value $r < 0$ can be set by the user in order to obtain the roots, $\Re(\lambda) \geq r$. For practical reasons, the steplength

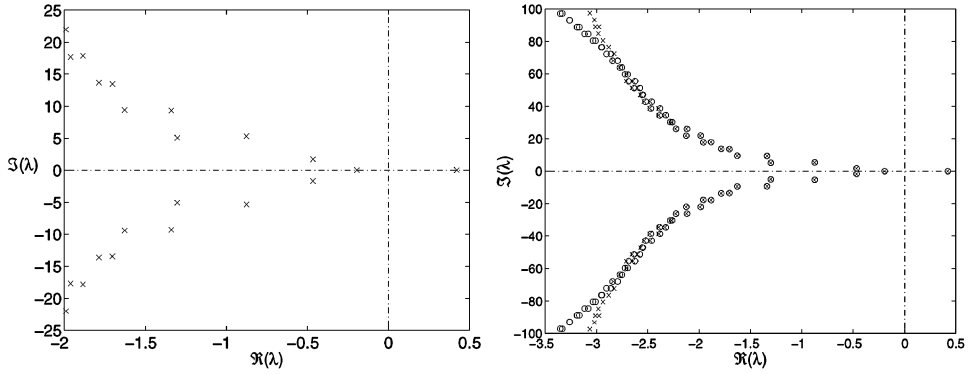

Fig. 3. Left: Correctly computed rightmost characteristic roots of (20), at $(x_1^*, x_2^*) = (0, 0)$, $a_{21} = 2.5$, $\tau_s = 1.5$. Roots were computed up to $\Re(\lambda) \geq -2$. Right: Approximated ($\circ$) and corrected ($\times$) characteristic roots of (20), at $(x_1^*, x_2^*) = (0, 0)$, $a_{21} = 2.5$, $\tau_s = 1.5$. Roots were computed up to $\Re(\lambda) \geq -3.5$.

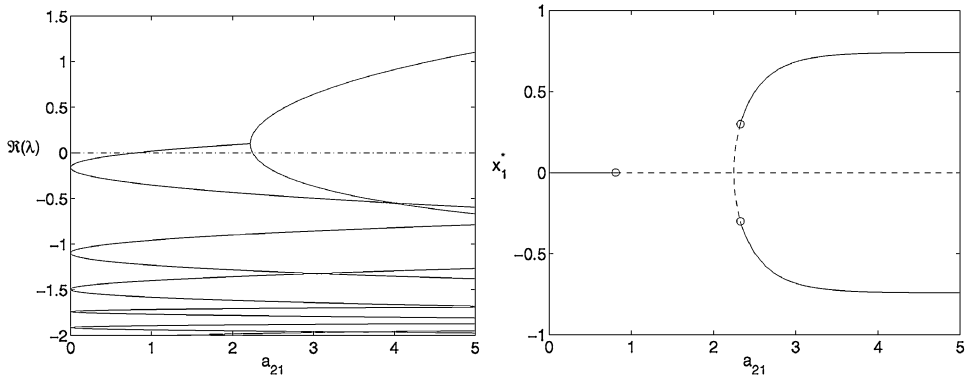

Fig. 4. Left: Real part of the characteristic roots of (20) along $(x_1^*, x_2^*) = (0, 0)$ versus a_{21} for $\tau_s = 1.5$. Right: Branches of steady state solutions of (20) undergoing Hopf bifurcations ($\circ$) and a pitchfork bifurcation. Stable and unstable parts of the branches denoted by solid, respectively, dashed lines.

h used to approximate the characteristic roots (cf. Section 3.1.2) is restricted from below (where, of course, the particular bound can be changed whenever required). If this bound is reached, a warning signals that approximated and corrected roots may diverge, possibly causing part of the wanted spectrum to be missed—see Figure 3 (right).

Figure 4 (left) depicts the stability along the constant zero branch versus a_{21} for $\tau_s = 1.5$. From this figure, it is not immediately clear which lines correspond to real roots or complex pairs of roots with the same real part. This can easily be decided upon by drawing figures like Figure 3. The zero steady state solution loses stability at a Hopf bifurcation near $a_{21} \approx 0.8071$, $\tau_s = 1.5$ and further undergoes a pitchfork bifurcation at $a_{21} = 2.25$, $\tau_s = 1.5$. The intersecting branch of nonzero solutions is shown in Figure 4 (right). Its stability is depicted in Figure 5 (left) versus x_1^* and shows the existence of two symmetrically placed Hopf bifurcations.

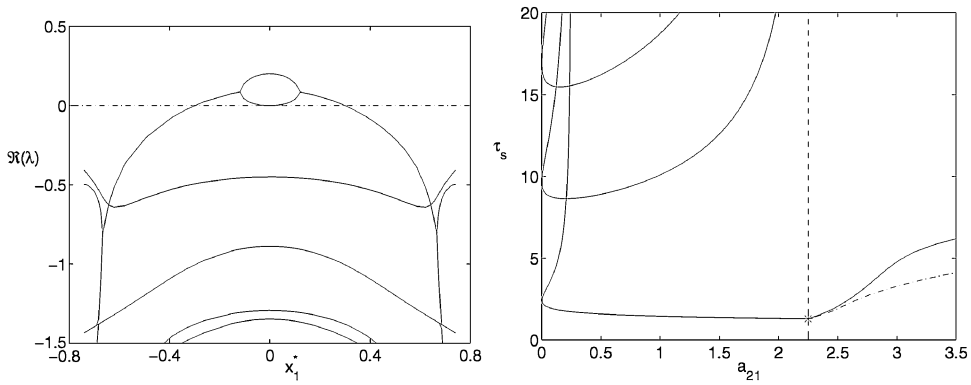

Fig. 5. Left: Real part of rightmost characteristic roots along the nonzero branch. Right: Branches of Hopf bifurcation points (−), branch of pitchfork bifurcation points (−−), Bogdanov-Takens point (∗) and branch of homoclinic solutions (·−) of (20). To the left of the branch of pitchfork bifurcation points, Hopf points belong to the zero steady state solution, to the right of this line, Hopf points correspond to the nonzero steady state solution.

In the (a_{21}, τ_s)-plane, the branch of pitchfork bifurcation points is just a vertical line, see Figure 5 (right). This is because the position of the pitchfork bifurcation is independent of the delays. The branch was computed by adding the symmetry condition (here $x_1 = 0$) to the determining system for a fold point. Because of the added condition, the resulting determining system is nonsquare (i.e. it is overdetermined) and is solved using a least squares approach as signalled by a warning (cf. Section 3.1.1). Due to the (nongeneric) symmetry, the extended system has isolated solutions.

Branches of Hopf bifurcation points for both the zero and the nonzero steady state solutions are depicted in Figure 5 (right). Both branches end in the same Bogdanov-Takens point located on the branch of pitchfork bifurcations. This and the occurrence of double Hopf points can be concluded by monitoring the rightmost characteristic roots along the branch of Hopf bifurcations, depicted (for the zero steady state solution) in Figure 6. At a double Hopf point one can switch to the intersecting branch of Hopf bifurcations associated with the second pair of purely imaginary eigenvalues. The intersecting branches of Hopf bifurcations shown in Figure 5 (right) were computed in this way.

During computation of periodic solution branches, the (user specified) degree of collocation polynomials and the number of subintervals remain fixed. By default, a mesh adaptation is applied every third point. If difficulties are encountered, the mesh should be refined and mesh adaptation can be applied every point. Such a situation can be signalled by an increase in the number of failures with respect to the number of successful corrections causing a steady decrease in the steplengths taken; by an apparent loss of smoothness of the computed branch and/or of the computed solutions, and by a loss of accuracy of the computed trivial multiplier. Some of these indications can also be caused by other phenomena, such as a steplength decrease due to a sharp turn in the branch, and an inaccurate trivial multiplier due to additional multipliers in the neighbourhood of 1.

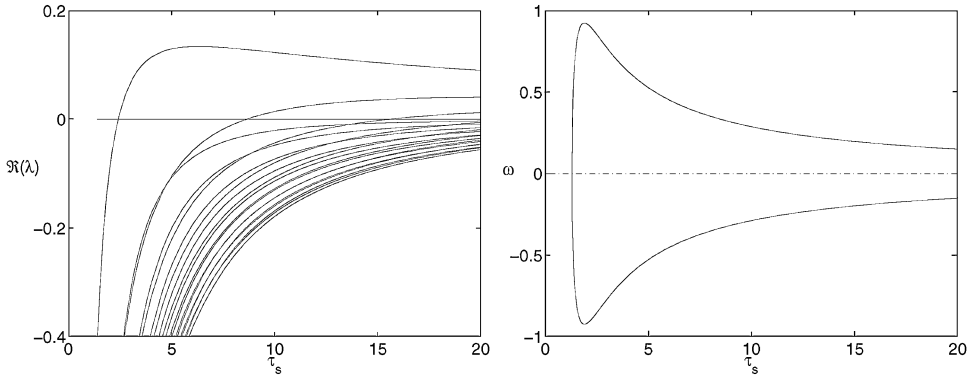

Fig. 6. Left: Real part of characteristic roots of the zero solution of (20) along the branch of Hopf bifurcation points emanating from the Bogdanov-Takens point shown in Figure 5 (right). Right: The frequency of the Hopf bifurcations along the same branch.

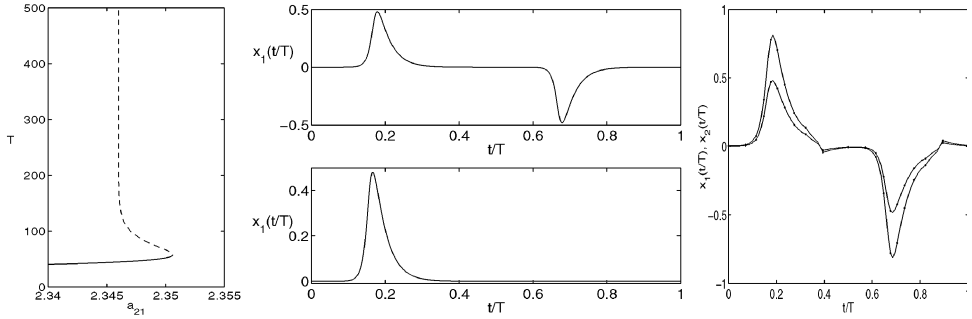

Fig. 7. Left: Period along a part of the branch of periodic solutions emanating from the Hopf point of the zero steady state solution of (20) versus a_{21} for $\tau_s = 1.5$. Stable and unstable parts of the branch are denoted by solid, respectively, dashed lines. Middle: Profiles of two periodic solutions approximating a double homoclinic (top) and normal homoclinic (bottom) solutions. For both profiles, period $T = 300$, $\tau_s = 1.5$, $a_{21} \approx 2.3460$. Right: Nonsmooth profile computed using a coarse mesh with $d = 3$ and $L = 20$.

The branch of periodic solutions which emanates from the Hopf point of the zero steady state branch for $\tau_s = 1.5$ is initially stable, looses stability in a turning point, and approaches a double homoclinic loop (due to symmetry). Its period is depicted in Figure 7 (left); a solution profile is depicted in Figure 7 (middle, top). The symmetric branches of periodic solutions that emanate from the nonzero steady state branches are always unstable. As a_{21} grows, both branches approach a (normal) homoclinic solution (see Figure 7 (middle, bottom)) which corresponds to the symmetric halves of the double homoclinic solution approached from the other side by the periodic solutions emanating from the zero steady state solution—see Figure 8.

As the periodic solutions approximate the homoclinic solution, computations were restarted with finer meshes (L was increased from 20 to 40 and d from 3 to 4). In this case, all criteria mentioned above apply and a computed

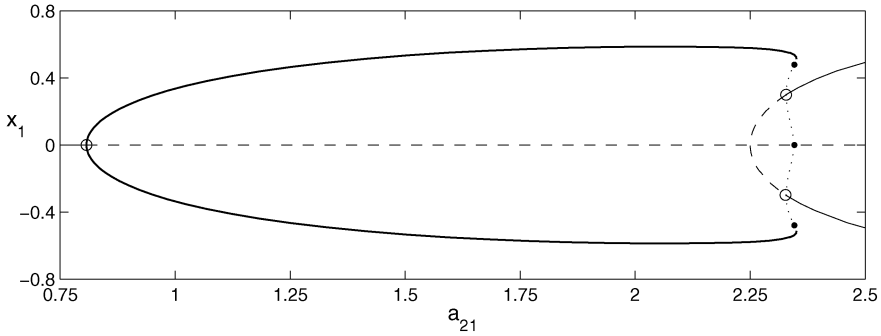

Fig. 8. Branches of stable (thin lines) and unstable (−−) steady state solutions as shown in Figure 4 (right). Hopf bifurcations (○) and minimum and maximum of $x_1(t)$ over the stable (thick lines) and unstable (···) branches of periodic solutions emanating from these Hopf bifurcations. The branch of periodic solutions emanating from the zero steady state solution looses stability in a turning point and subsequently approaches a double homoclinic orbit (•). The symmetric branches of periodic solutions emanating from the nonzero steady state solutions are always unstable and each approach a homoclinic orbit (•) which is half of the double homoclinic orbit.

Table I. Approximated, Corrected and Exact Characteristic Roots for the Zero Steady State Solution of (20) at $a_{21} = 1e-8$, $\tau_s = 1.5$

	approximated roots	corrected roots	exact roots
$\lambda_{1,2}$	$-0.16081 \pm 1.2270i$	$-0.16091 \pm 1.2270i$	$-0.16088 \pm 1.2269i$
$\lambda_{3,4}$	$-0.16085 \pm 1.2271i$	$-0.16091 \pm 1.2270i$	$-0.16091 \pm 1.2270i$

nonsmooth solution indicating that a finer mesh is needed is depicted in Figure 7 (right).

A branch of homoclinic solutions in two-parameter space can be approximated by a branch of periodic solutions with fixed, large period. We add the extra condition $T = 300$ and free a second parameter, τ_s. The computed branch, see Figure 5 (right), emanates nontangentially from the Bogdanov-Takens point. This behaviour does not completely correspond with the normal form analysis of a Bogdanov-Takens point (for a system of ordinary differential equations, see, e.g., Kuznetsov [1995, §VIII.4.2]) probably due to the extra symmetry involved here .

If the parameter a_{21} is set to zero, one of the connections between the neurons is absent and all characteristic roots appear double. This does not produce any problems. However, for small values of a_{21} the spectrum consists of pairs of nearby roots. Here, we could observe—see Table I—the occurrence of two different approximated roots being corrected to the same exact root by the Newton's iteration. In this way, part of the spectrum is missed by the corrections. For this reason, approximations and corrections should best be compared. We note, however, that the situation here is rather special and, considering the distance between the exact roots, one could say that the two equal corrected roots still form a reasonable approximation of the exact spectrum. During other tests, we did not encounter problems of this nature.

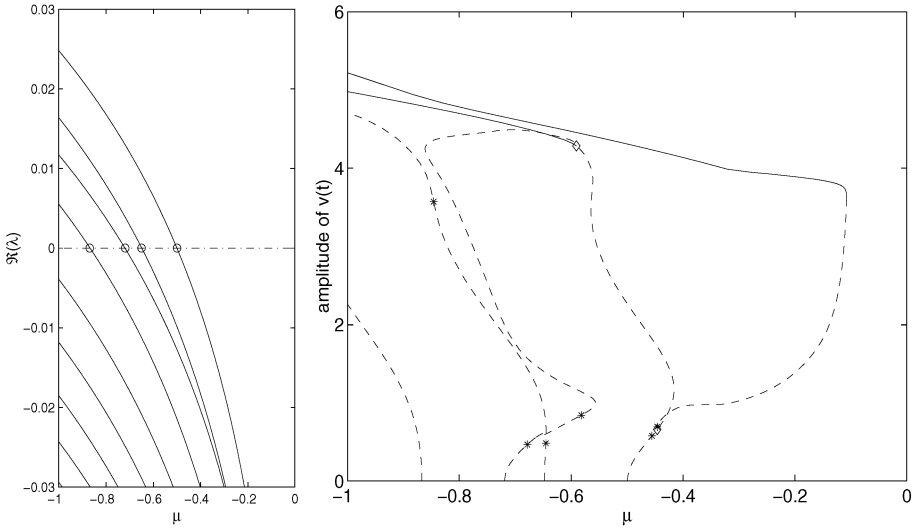

Fig. 9. Left: Real part of the rightmost roots of the characteristic equation along the solution branch (v^*, w^*) of (21) for varying μ. All depicted roots consist of complex pairs and four Hopf bifurcations ($\circ$) occur. Right: Amplitude of $v(t)$ along the emanating branches of periodic solutions. Stable branches (—), unstable branches (−−). Several torus bifurcations ($*$), turning points and two period doubling bifurcations ($\diamond$) were detected. The period doubled branches are also shown.

4.2 Example 2

The following model describes recurrent neural feedback and was analysed in Plant [1981] and Castelfranco and Stech [1987],

$$\begin{cases} \dot{v}(t) = h(v(t)) - w(t) + \mu(v(t-\tau) - v^*) \\ \dot{w}(t) = \rho(v(t) + a - bw(t)), \end{cases} \tag{21}$$

where $h(v) = v - \frac{1}{3}v^3$, $a = 0.7$, $b = 0.8$, $\rho = 0.08$, $\tau = 25$ and $v^* \approx -1.1994$ is the unique real root of $h(v^*) - (v^* + a)/b = 0$ which, together with $w^* = (v^* + a)/b$ corresponds to an equilibrium of the system.

Stability along the constant (v^*, w^*) steady state branch is shown in Figure 9 (left) versus μ. Four Hopf bifurcations are visible. The emanating branches of periodic solutions are depicted in Figure 9 (right). Several bifurcations (turning points, torus bifurcations, and period doubling bifurcations) were found and detected using appropriate visualisation of the computed Floquet multipliers.

The stability results—Figure 9 (right)—differ partially from the ones obtained in Castelfranco and Stech [1987], where the periodic solutions are computed using Fourier approximation. This is probably caused by the steep gradients in the solutions, which are not easily captured using this type of approximation. Convergence of the computed period and Floquet multipliers for a periodic solution with steep gradients is illustrated in Tables II and III. Note that the accuracy of the trivial multiplier is not a good indication of the accuracy of the other multipliers (whose corresponding eigenfunctions may differ greatly). For Figure 9 (right), we used collocation polynomials of degree $d = 3, 4$

Table II. Convergence of the Period and Dominant Floquet Multipliers for a Stable Periodic Solution at $\mu = -2$ on Uniform Meshes as the Mesh is Refined

L	T	$\lvert\mu_1 - 1\rvert$	$\mu_{2,3}$
10	50.23794	$1.3e+0$	0.14433
20	50.47178	$1.7e+0$	$0.20480 \pm 0.04283i$
40	50.78587	$2.7e-2$	$0.13953 \pm 0.04233i$
80	50.72830	$2.4e-2$	$0.14449 \pm 0.03806i$
160	50.73267	$1.4e-3$	$0.14439 \pm 0.03820i$

Table III. Convergence of the Period and Dominant Floquet Multipliers for a Stable Periodic Solution at $\mu = -2$ on Adapted Meshes as the Mesh is Refined

L	T	$\lvert\mu_1 - 1\rvert$	$\mu_{2,3}$
10	50.56190277	$2.8e+1$	$0.21162 \pm 0.05819i$
20	50.73279409	$1.0e-2$	$0.16182 \pm 0.01437i$
40	50.73262760	$5.1e-5$	$0.14179 \pm 0.04098i$
80	50.73262554	$3.3e-6$	$0.14506 \pm 0.03884i$
160	50.73262542	$1.1e-6$	$0.14437 \pm 0.03817i$

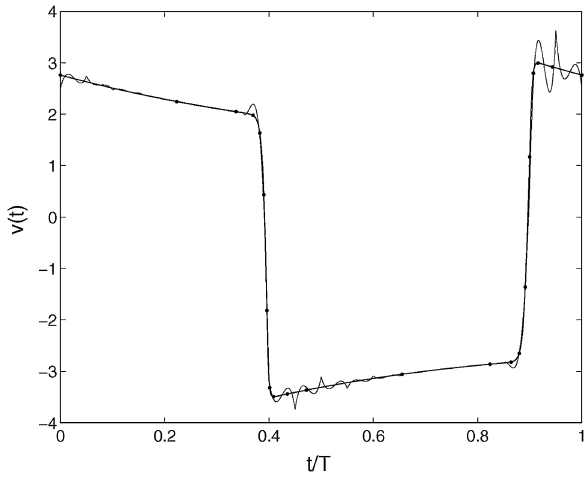

Fig. 10. Computed stable periodic solution of (21) at $\mu = -2$ using $L = 20$, $d = 3$ and an equidistant (thin line) or an adapted (thick line) mesh. Unphysical oscillations near steep gradients are computed on the uniform mesh when the subinterval size is not fine enough.

on adapted meshes with $L = 40, 50$ subintervals. The effectiveness of the mesh adaptation is further illustrated in Figure 10.

4.3 Example 3

The following model of two linearly coupled oscillators was studied in Reddy et al. [1998, 1999],

$$\begin{cases} \dot{Z}_1(t) = (1 + \mathrm{i}\omega_1 - |Z_1(t)|^2)Z_1(t) + K(Z_2(t-\tau) - Z_1(t)) \\ \dot{Z}_2(t) = (1 + \mathrm{i}\omega_2 - |Z_2(t)|^2)Z_2(t) + K(Z_1(t-\tau) - Z_2(t)). \end{cases} \tag{22}$$

Here, Z_j is the complex amplitude of the j-th oscillator and $K \geq 0$ is the coupling strength.

Phase locked solutions in which the two oscillators synchronise to a common frequency B, can be described by the representation

$$(Z_1(t), Z_2(t)) \equiv \left(r_1 e^{i(Bt-\alpha/2)}, r_2 e^{i(Bt+\alpha/2)}\right), \tag{23}$$

where r_1, r_2, α and B are real constants. For $\tau \neq 0$, there is a rich set of such solutions. In [Reddy et al. 1999], solutions of type (23) were tracked numerically by solving a polar representation of (22) together with (23) for varying parameter K. The stability of the obtained solutions was studied through the analysis of the characteristic equation and time integration of the original system for a number of parameter values.

Phase locked solutions can be computed and analysed as steady state solutions using the substitution,

$$Z_j(t) = \tilde{Z}_j(t) e^{iBt}, \quad j = 1, 2. \tag{24}$$

This is possible, because, due to the special structure of the equations, terms e^{iBt} drop out and a new autonomous system of equations is obtained. For the same reason, if $(Z_1^a(t), Z_2^a(t)) \equiv (r_1(t)e^{ip_1(t)}, r_2(t)e^{ip_2(t)})$ is a solution then so is $(Z_1^b(t), Z_2^b(t)) \equiv (r_1(t)e^{i(p_1(t)+\Delta p)}, r_2(t)e^{i(p_2(t)+\Delta p)})$ for any (constant) Δp. To remove this indeterminacy we add an extra condition,

$$\Im(\tilde{Z}_1(0)) = 0. \tag{25}$$

In the real variables $x_j(t) = \Re(\tilde{Z}_j(t))$, $y_j(t) = \Im(\tilde{Z}_j(t))$ $(j = 1, 2)$ and B, system (22) has the form,

$$\begin{cases} \dot{x}_1(t) = B y_1(t) + x_1(t)(1 - x_1(t)^2 - y_1(t)^2) - \omega_1 y_1(t) \\ \qquad + K(x_2(t-\tau)\cos(-B\tau) - y_2(t-\tau)\sin(-B\tau) - x_1(t)) \\ \dot{y}_1(t) = -B x_1(t) + y_1(t)(1 - x_1(t)^2 - y_1(t)^2) + \omega_1 x_1(t) \\ \qquad + K(y_2(t-\tau)\cos(-B\tau) + x_2(t-\tau)\sin(-B\tau) - y_1(t)) \\ \dot{x}_2(t) = B y_2(t) + x_2(t)(1 - x_2(t)^2 - y_2(t)^2) - \omega_2 y_2(t) \\ \qquad + K(x_1(t-\tau)\cos(-B\tau) - y_1(t-\tau)\sin(-B\tau) - x_2(t)) \\ \dot{y}_2(t) = -B x_2(t) + y_2(t)(1 - x_2(t)^2 - y_2(t)^2) + \omega_2 x_2(t) \\ \qquad + K(y_1(t-\tau)\cos(-B\tau) + x_1(t-\tau)\sin(-B\tau) - y_2(t)) \end{cases} \tag{26}$$

and condition (25) is equivalent to

$$y_1(0) = 0. \tag{27}$$

Using system (26) and (27) as an extra condition, we computed a branch of steady state solutions and an emanating branch of periodic solutions—see Figure 11. Note that the branches are depicted with respect to the variables $r_j(t) = |\tilde{Z}_j(t)|$ $(j = 1, 2)$. The non-smoothness of the branch in Figure 11 (left) is due to the fact that $r_1(\tilde{t}) = 0$ at some $\tilde{t} \in [0, T]$ when $K \approx 0.6902$. Such a point cannot easily be passed using a polar representation, and this is why we preferred the cartesian representation (26). The branch of periodic solutions is initially stable but looses stability in a turning point. Remark that such a periodic solution is actually quasi-periodic in terms of the original variables

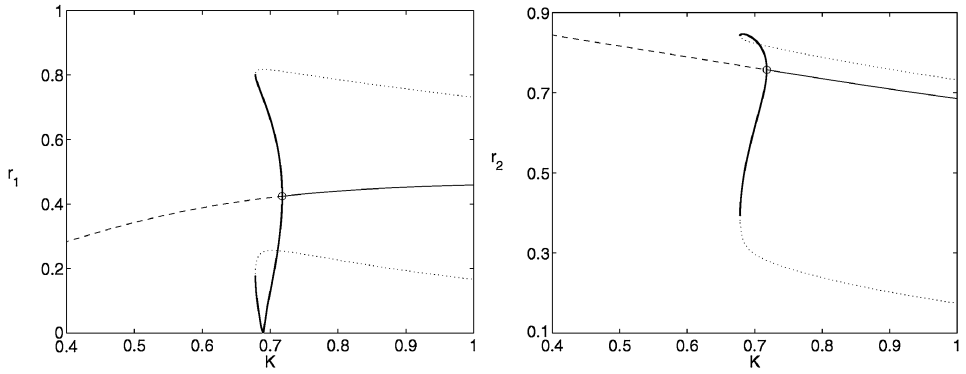

Fig. 11. Branches of steady state and periodic solutions (maximum and minimum values of r_j) of (26) for $\omega_1 = 10.5, \omega_2 = 9.5$, $\tau \approx 0.4714$. Stable (thin lines) and unstable ($--$) branches of steady state solutions and stable (thick lines) and unstable ($\cdots$) branches of periodic solutions, Hopf bifurcation ($\circ$).

$(Z_1(t), Z_2(t))$. One frequency is present in the periodicity of $(x_j(t), y_j(t))$, $j = 1, 2$. The other is present in the parameter $B \neq 0$ through (24).

5. CONCLUDING COMMENTS

The aim of DDE-BIFTOOL is to provide a portable, user-friendly tool for numerical bifurcation analysis of steady state solutions and periodic solutions of systems of delay equations with several fixed discrete delays. Part of this goal was fulfilled through choosing the portable, programmer-friendly environment offered by Matlab. Furthermore, whenever possible, the user is shielded off from numerical details. This is achieved through the availability of default method parameters, through automatic steplength selection in approximating the rightmost characteristic roots and through the use of adaptive mesh selection for the computation of periodic solutions.

Although there are no 'hard' limits programmed in the package (with respect to system and/or mesh sizes), the user will notice the rapidly increasing computation time for increasing system dimension and mesh sizes. This exhibits itself most profoundly in the stability and periodic solution computations. Indeed, eigenvalues are computed and the Newton procedure on periodic solutions is implemented without exploiting the sparsity present in the large matrices used. Nevertheless the current version is sufficient to perform bifurcation analysis of systems with reasonable properties in reasonable execution times.

Future plans include more efficient linear algebra procedures, a graphical user interface and the extension to other types of delay equations (such as distributed delay and neutral functional differential equations).

REFERENCES

ASCHER, U. M., MATTHEIJ, R. M. M., AND RUSSELL, R. D. 1988. *Numerical Solution of Boundary Value Problems for Ordinary Differential Equations*. Prentice Hall.

CASTELFRANCO, A. M. AND STECH, H. W. 1987. Periodic solutions in a model of recurrent neural feedback. *SIAM J. Appl. Math. 47*, 3, 573–588.

CORWIN, S. P., SARAFYAN, D., AND THOMPSON, S. 1997. DKLAG6: A code based on continuously imbedded sixth order Runge-Kutta methods for the solution of state dependent functional differential equations. *Appl. Numer. Math. 24*, 2–3, 319–330.

DIEKMANN, O., VAN GILS, S. A., VERDUYN LUNEL, S. M., AND WALTHER, H.-O. 1995. *Delay Equations: Functional-, Complex-, and Nonlinear Analysis*. Applied Mathematical Sciences, vol. 110. Springer-Verlag.

DOEDEL, E. J., CHAMPNEYS, A. R., FAIRGRIEVE, T. F., KUZNETSOV, Y. A., SANDSTEDE, B., AND WANG, X. 1997. AUTO97: Continuation and bifurcation software for ordinary differential equations; available via ftp.cs.concordia.ca in directory pub/doedel/auto.

DOEDEL, E. J., KELLER, H. B., AND KERNEVEZ, J. P. 1991a. Numerical analysis and control of bifurcation problems (I) bifurcation in finite dimensions. *Internat. J. Bifur. Chaos 1*, 3, 493–520.

DOEDEL, E. J., KELLER, H. B., AND KERNEVEZ, J. P. 1991b. Numerical analysis and control of bifurcation problems (II) bifurcation in infinite dimensions. *Internat. J. Bifur. Chaos 1*, 4, 745–772.

ENGELBORGHS, K. 2000a. DDE-BIFTOOL: a Matlab package for bifurcation analysis of delay differential equations. Tech. Rep. TW-305, Department of Computer Science, K. U. Leuven, Leuven, Belgium. Available from http://www.cs.kuleuven.ac.be/~koen/delay/ddebiftool.shtml.

ENGELBORGHS, K. 2000b. Numerical bifurcation analysis of delay differential equations. Ph.D. dissertation, Dep. of Computer Science, K. U. Leuven, Leuven, Belgium.

ENGELBORGHS, K. AND DOEDEL, E. 2001. Stability of piecewise polynomial collocation for computing periodic solutions of delay differential equations. Numerische Mathematik; DOI 10.1007/S002110100313.

ENGELBORGHS, K., LUZYANINA, T., IN ´T HOUT, K. J., AND ROOSE, D. 2000a. Collocation methods for the computation of periodic solutions of delay differential equations. *SIAM J. Sci. Comput. 22*, 5, 1593–1609.

ENGELBORGHS, K., LUZYANINA, T., AND ROOSE, D. 2000b. Numerical bifurcation analysis of delay differential equations. *J. Comput. Appl. Math. 125*, 1–2, 265–275.

ENGELBORGHS, K., LUZYANINA, T., AND SAMAEY, G. 2001. DDE-BIFTOOL v. 2.00: a Matlab package for bifurcation analysis of delay differential equations. Tech. Rep. TW-330, Department of Computer Science, K. U. Leuven, Leuven, Belgium. Available from http://www.cs.kuleuven.ac.be/~koen/delay/ddebiftool.shtml.

ENGELBORGHS, K. AND ROOSE, D. 1999. Numerical computation of stability and detection of Hopf bifurcations of steady state solutions of delay differential equations. *Adv. Comput. Math. 10*, 3–4, 271–289.

ENGELBORGHS, K. AND ROOSE, D. 2001. On stability of LMS-methods and characteristic roots of delay differential equations. *SIAM J. Num. Analysis*.

ERMENTROUT, B. 1998. *XPPAUT3.91—The differential equations tool*. University of Pittsburgh, Pittsburgh. (http://www.pitt.edu/~phase/).

GOVAERTS, W. 2000. *Numerical Methods for Bifurcations of Dynamical Equilibria*. SIAM.

HAIRER, E., NORSETT, S. P., AND WANNER, G. 1993. *Solving ordinary differential equations. 1: Nonstiff problems*, 2nd ed. Springer series in computational mathematics, vol. 8. Springer Berlin.

HALE, J. K. 1977. *Theory of Functional Differential Equations*. Applied Mathematical Sciences, vol. 3. Springer-Verlag.

HALE, J. K. AND VERDUYN LUNEL, S. M. 1993. *Introduction to Functional Differential Equations*. Applied Mathematical Sciences, vol. 99. Springer-Verlag.

HASSARD, B. D. 1987. A code for Hopf bifurcation analysis of autonomous delay-differential systems. In *Oscillations, Bifurcations and Chaos*, F. V. Atkinson, W. F. Langford, and A. B. Mingarelli, Eds. Can. Math. Soc. Conference Proceedings, vol. 8. Amer. Math. Soc., Providence, RI, 447–463.

HONG-JIONG, T. AND JIAO-XUN, K. 1996. The numerical stability of linear multistep methods for delay differential equations with many delays. *SIAM J. Numer. Anal. 33*, 3, 883–889.

KOLMANOVSKII, V. B. AND MYSHKIS, A. 1999. *Introduction to the Theory and Application of Functional Differential Equations*. Mathematics and its Applications, vol. 463. Kluwer Academic Publishers.

KUZNETSOV, Y. A. 1995. *Elements of Applied Bifurcation Theory*. Applied Mathematical Sciences, vol. 112. Springer-Verlag.

LUZYANINA, T. AND ENGELBORGHS, K. 2001. Computing Floquet multipliers for functional differential equations. *Internat. J. Bifur. Chaos*.

LUZYANINA, T. AND ROOSE, D. 1996. Numerical stability analysis and computation of Hopf bifurcation points for delay differential equations. *J. Comput. Appl. Math. 72*, 379–392.

PAUL, C. A. H. 1997. A user-guide to Archi—an explicit Runge-Kutta code for solving delay and neutral differential equations. Tech. Rep. 283, The University of Manchester, Manchester Center for Computational Mathematics.

PLANT, R. E. 1981. A FitzHugh differential-difference equation modeling recurrent neural feedback. *SIAM J. Appl. Math. 40*, 1, 150–162.

REDDY, D. V. R., SEN, A., AND JOHNSTON, G. L. 1998. Time delay induced death in coupled limit cycle oscillators. *Phys. Rev. Lett. 80*, 5109–5112.

REDDY, D. V. R., SEN, A., AND JOHNSTON, G. L. 1999. Time delay effects on coupled limit cycle oscillators at Hopf bifurcation. *Physica D 129*, 15–34.

SEYDEL, R. 1994. *Practical Bifurcation and Stability Analysis—From Equilibrium to Chaos*, 2nd ed. Interdisciplinary Applied Mathematics, vol. 5. Springer-Verlag Berlin.

SHAYER, L. P. AND CAMPBELL, S. A. 2000. Stability, bifurcation and multistability in a system of two coupled neurons with multiple time delays. *SIAM J. Appl. Math. 61*, 2, 673–700.

Received January 2001; revised February 2002; accepted February 2002